Hyperfine interaction of Er^{3+} ions in Y_2SiO_5: An electron paramagnetic resonance spectroscopy study

O. Guillot-Noël,* Ph. Goldner, and Y. Le Du
Laboratoire de Chimie de la Matière Condensée de Paris, CNRS-UMR 7574, ENSCP, 11 rue Pierre et Marie Curie, 75231 Paris Cedex 05, France

E. Baldit, P. Monnier, and K. Bencheikh
Laboratoire de Photonique et Nanostructures, CNRS-UPR 20, Route de Nozay, 91 460 Marcoussis, France
(Received 11 July 2006; revised manuscript received 23 October 2006; published 11 December 2006)

Electron paramagnetic resonance (EPR) spectroscopy of rare earth ions in crystals is a powerful tool to analyze the hyperfine structure of the rare earth ground state. This can be useful for coherent spectroscopy and quantum information applications where the hyperfine structure of the electronic levels is used. In this work, we give a detailed analysis of the hyperfine structure of the ground state $[^4I_{15/2}(0)]$ of Er^{3+} ions in Y_2SiO_5. The electronic Zeeman, hyperfine, and quadrupole matrices are obtained from angular variations of the magnetic field in three orthogonal crystal planes. An excellent agreement is obtained between experimental and simulated magnetic field positions and relative intensities of EPR lines.

DOI: 10.1103/PhysRevB.74.214409 PACS number(s): 76.30.−v, 31.30.Gs

I. INTRODUCTION

Hyperfine levels of rare earth ions are commonly used to perform coherent spectroscopy experiments, like hole burning and photon echo, thanks to the long lifetime (up to minutes) of these levels at low temperature (<4 K).[1] They can also exhibit a coherence time (T_2) of the order of several milliseconds, making these systems interesting for quantum manipulations. For example, a hyperfine coherence lifetime of 82 ms has been reported in $Pr^{3+}:Y_2SiO_5$.[2] By the application of a specific pulse sequence on a nuclear-quadrupole transition of Pr^{3+} ions, an increase of up to 30 s has been found for this coherence time.[3] Rare-earth-ion-doped crystals are thus promising candidates in the quest for macroscopic quantum effects like quantum memories[4] and quantum repeaters.[5] In both applications, quantum storage, which aims at transferring quantum states of photons into atomic ensembles, is necessary. This is possible with atomic species in which a three-level Λ system can be built.[6] A three-level Λ system consists of two levels, which can both be coupled by light fields to a third one. The photon to be stored is resonant with one transition and a second light field with the other one. Intensity variation of the latter allows photons to be trapped and released by using electromagnetically induced transparency (EIT) for example.[6] To get efficient trapping, the lifetime of the coherences (optical and hyperfine coherences) between the three levels of the Λ system needs to be long. The hyperfine coherence time defines the storage time of the quantum memory. Storage has been demonstrated for classical and quantum light in a number of systems.[4,7,8] In $Pr^{3+}:Y_2SiO_5$, light was slowed down and even stopped during a time span greater than one second.[9] In this case, the three-level system is made of the hyperfine levels of the ground $^3H_4$ multiplet and of the excited $^1D_2$ multiplet of Pr^{3+} ions.

Apart from the required long coherence time, the two optical transitions between the two legs of the Λ should have similar intensities. This condition is satisfied if the nuclear spin projection M_I is not a good quantum number since optical transitions are limited by the $\Delta M_I=0$ selection rule. In order to find an efficient three-level Λ system with hyperfine levels of rare earth ions, some mixing between the $|M_I\rangle$ states has to occur. There are two ways to induce mixing in the nuclear spin projections: (i) to find a host where the site symmetry of the rare earth is low and/or (ii) to apply an external magnetic field. In the former case, hyperfine interaction in low symmetry sites induces mixing between $|M_I\rangle$ and $|M_I\pm1\rangle$ states and quadrupole interaction mixes state $|M_I\rangle$ and $|M_I\pm2\rangle$. In the latter case, in previous works on Pr^{3+} and Tm^{3+} ions, we have shown theoretically and experimentally that an external magnetic field can induce very different nuclear spin projections by mixing ground and excited levels and thus relaxing the $\Delta M_I=0$ selection rule.[10–12]

In the future, quantum networks will be composed of photons as natural qubit carriers and atomic systems as nodes for processing and storing the optical information. Finding suitable atomic systems and protocols meeting the current telecommunication technologies appears as a crucial point. In this perspective, Er^{3+} ion belongs to the family of rare earths showing very sharp optical resonances with long-lived excited states and long optical coherence times. Among all the rare earth ions, non-Kramers ions with an even number of $4f$ electrons present the longest coherence lifetime without any magnetic field.[13] However, under an external magnetic field, Kramers ions, like Er^{3+}, can also be of interest. An optical coherence lifetime of 4.38 ms has been obtained in $Er^{3+}:Y_2SiO_5$ under magnetic field corresponding to the longest optical coherence time ever measured in any solid-state material.[14] Er^{3+} ion is an interesting Kramers ion as it emits around 1.5 μm. The presence of telecommunication optical fibers makes this wavelength suitable to transfer light qubits over long distances. Moreover, Er^{3+} ions present a hyperfine structure at zero magnetic field due to the ^{167}Er isotope (natural abundance 22.94%) with a nuclear spin $I=7/2$. A three-level Λ system can be built between the hyperfine levels of the ground $^4I_{15/2}$ multiplet and of the excited $^4I_{13/2}$

multiplet around 1.5 μm. Y_2SiO_5 has a monoclinic structure with $C2/c$ space group. Er^{3+} ions lie on two crystallographic sites with low-symmetry C_1 with seven and six oxygen neighbors. This low site symmetry induces strong mixing between the different nuclear spin projections. For all the above reasons, $Er^{3+}:Y_2SiO_5$ appears to be an interesting candidate for light processing and storing.

The first step toward coherent optical applications and quantum manipulation in this system is the determination of the hyperfine structure of the ^{167}Er isotope in Y_2SiO_5. Because of the very low site symmetry of the rare earth, each Kramers doublet of this isotope splits at maximum into 16 levels under the hyperfine and quadrupole magnetic interactions even without any external magnetic field. The hyperfine structure of Er^{3+} ions is thus very complex. As the hyperfine splittings (few hundreds of megahertz) are usually smaller than the optical inhomogeneous linewidth (few gigahertz), they can only be determined in the optical range by hole burning spectroscopy. However, due to the high value of the nuclear spin of the ^{167}Er isotope ($I=7/2$), hole burning spectra are very complex. If we consider that the hyperfine splittings are inside the inhomogeneous linewidth and if all the transitions are allowed, we have at maximum 2×120 side holes and $2\times28\ 800$ antiholes. In this very complex case, electron paramagnetic resonance (EPR) spectroscopy is a powerful tool to analyze the hyperfine structure of the ground Kramers doublet of the $^4I_{15/2}$ multiplet. Although limited to the ground state crystal field level, this technique has two main advantages over its optical counterpart. First, the inhomogeneous linewidth of the Zeeman transitions in rare earth ions is approximately three orders of magnitudes smaller than those observed in the optical domain. This allows one to observe very clearly splittings due to different interactions as the hyperfine and quadrupole ones. Moreover, by rotating a single crystal in the magnetic field, precise information on the site symmetry (including ground state irreducible representation), and also on the orientation of the different interactions can be easily retrieved. This can be used in order to optimize the hyperfine states mixing and the coherence time when an external magnetic field is applied.

Having determined the ground state hyperfine splitting by EPR, hole burning spectroscopy could then be used to retrieve the excited state hyperfine structure. Apart from the determination of hyperfine splittings for quantum applications, the EPR of Er^{3+} ions in Y_2SiO_5 provides an interesting case for the study of low-symmetry effects in electron paramagnetic resonance. Indeed, low-symmetry EPR data are difficult to interpret as the different interactions, the Zeeman interaction, the hyperfine interaction and the quadrupole interaction have noncoincident principal axes.[15] Moreover, under low site symmetry, second-order effects of hyperfine and quadrupole interactions can strongly modify the splitting between hyperfine transitions. To our knowledge, it is the first time that such a complete study of EPR spectra of Er^{3+} ions in low site symmetry is reported. Indeed, in the literature, very few examples of this type are studied. Only the **g** factor and the hyperfine interaction **A** are determined and very often the quadrupole interaction is neglected.[16]

The paper is arranged as follows. In Sec. II, we present the spin-Hamiltonian approach which is used to analyze the hyperfine splittings of the ground state of erbium as well as the fitting procedure used in this work. In Sec. III, the results and the spin-Hamiltonian parameters are presented and discussed.

II. SPIN HAMILTONIAN AND FITTING PROCEDURE

The free Er^{3+} ion has a $4f^{11}$ configuration with a $^{2S+1}L_J = {}^4I_{15/2}$ ground state. S, L, and J are the spin, orbital, and total momenta, respectively. In a crystal field of C_1 symmetry, the $J=15/2$ level splits into eight Kramers doublets (KDs) $|M_J|=15/2$, $13/2$, $11/2$, $9/2$, $7/2$, $5/2$, $3/2$, and $1/2$, M_J being the z component of J. Since only the lowest doublet is populated at liquid helium temperature, the system can be described by a fictitious spin $S=1/2$. Erbium has five even isotopes ^{162}Er, ^{164}Er, ^{166}Er, ^{168}Er, and ^{170}Er, with nuclear spin $I=0$ and a total natural abundance of 77.05%, and one isotope, ^{167}Er, with nuclear spin $I=7/2$ (natural abundance 22.95%). The EPR spectrum of Er^{3+} ions is expected to be composed of an intense central line due to even isotopes and a hyperfine pattern composed of at least eight "allowed" transitions for the odd isotope; "allowed" means that the EPR transition has the selection rules $\Delta M_S=\pm1$ and $\Delta M_I=0$. As the low site symmetry mixes all the nuclear spin projections, M_I is not a good quantum number anymore; however, it is simple to describe the EPR spectrum by means of allowed ($\Delta M_I=0$) and forbidden transitions ($\Delta M_I=\pm1,\pm2$). The spin Hamiltonian developed by Pryce[17] and Abragam and Pryce[18] using a modified perturbation theory is

$$H_{even}=\beta_e\mathbf{B}\cdot\mathbf{g}\cdot\mathbf{S} \tag{1}$$

for even isotopes and

$$H_{odd}=\beta_e\mathbf{B}\cdot\mathbf{g}\cdot\mathbf{S}+\mathbf{I}\cdot\mathbf{A}\cdot\mathbf{S}+\mathbf{I}\cdot\mathbf{Q}\cdot\mathbf{I}-\beta_n g_n\mathbf{B}\cdot\mathbf{I} \tag{2}$$

for the odd isotope. β_e is the electronic Bohr magneton, **B** is the external static magnetic field, **g** is the g-factor matrix, **A** is the hyperfine matrix, and **Q** is the electric quadrupole matrix. The quadrupole interaction is a symmetric traceless matrix. β_n is the nuclear magneton, and g_n is the nuclear g factor. $g_n=-0.1618$ for Er^{3+} ions.

The crystal used in our experiments is supplied by Scientific Materials Inc. A cube of 1 mm^3 is oriented by Laue x-ray diffraction along the three orthogonal optical extinction axes, $\boldsymbol{b}$, $\boldsymbol{D}_1$, and $\boldsymbol{D}_2$.[14] It is doped with 0.005 at. % of Er^{3+} ions. The EPR spectra of erbium-doped Y_2SiO_5 are shown in Fig. 1 for **B** parallel to $\boldsymbol{b}$ for example. The signals from the erbium ions in site 1 and site 2 are gathered. We use the notation of Refs. 14 and 19 site 1 (site 2) corresponds to Er^{3+} ions characterized by the 1536.48 nm (1538.90 nm) vacuum wavelength for the lowest $^4I_{15/2}$ to $^4I_{13/2}$ transitions.

The EPR spectra are composed of a narrow central line corresponding the even isotopes. A hyperfine pattern of $2I+1=8$ allowed hyperfine transitions ($\Delta M_I=0$ transitions which are indicated by a stick diagram on Fig. 1) is seen around the central line. Between each allowed hyperfine transition, pairs of forbidden transitions ($\Delta M_I=\pm1$ transitions, stick diagram on Fig. 1) are clearly observed. In a site of C_1 symmetry, the principal axes of each interaction **g**, **A**,

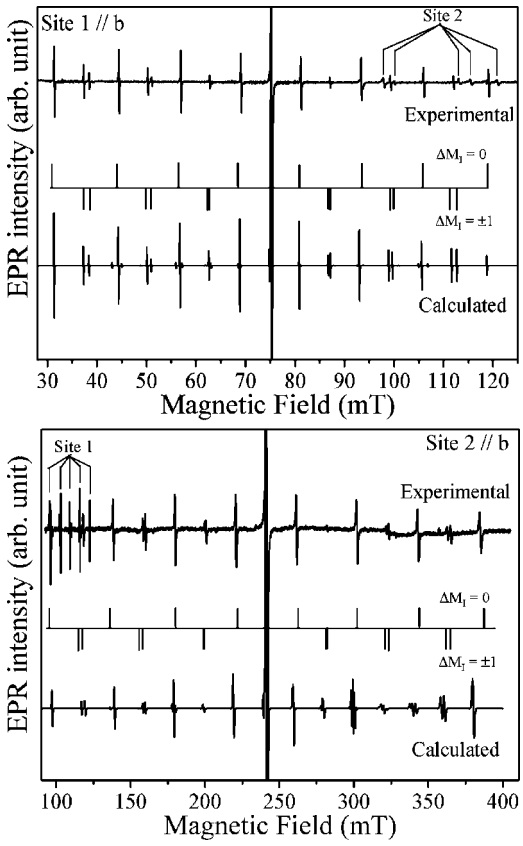

FIG. 1. Experimental and calculated EPR spectra at 7 K of Er^{3+} in Y_2SiO_5 for sites 1 and 2 with the magnetic field **B** parallel to the ***b*** axis. The spectra were recorded at 9.5 GHz with a microwave power of 20 mW.

Q are not coincident. The determination of **g**, **A**, and **Q** matrices with respect to a reference axis set is obtained from the angular variations of the experimental EPR spectra in three orthogonal crystal planes: $(\boldsymbol{b},\boldsymbol{D}_1)$, $(\boldsymbol{b},\boldsymbol{D}_2)$, and $(\boldsymbol{D}_1,\boldsymbol{D}_2)$. In the general case, **g** and **A** are asymmetric.[20] The asymmetric part of the **g** matrix can be eliminated by special spin operator transformation.[21] However, such an asymmetry has not be seen in our spectra and all matrices are taken symmetric. We have thus to determine 17 spin-Hamiltonian parameters: six for the **g** matrix, six for the **A** matrix, and only five for the **Q** matrix, which is a traceless matrix. The six **g**-factor matrix elements are obtained from the angular study of the central EPR line [Eq. (1)]. The other 11 parameters are obtained from angular variations of the allowed and forbidden transitions. Contrary to what is usually done, we cannot use a perturbative approach to analyze the hyperfine structure in the case of $Er^{3+}:Y_2SiO_5$. As the intensities of some forbidden hyperfine transitions are of the same order of magnitude as the allowed transitions (Fig. 1), the quadrupole interaction cannot be treated as a perturbation of the hyperfine interaction. It means that we have to perform a complete diagonalization of the spin Hamiltonian of Eq. (2) to retrieve the **A** and **Q** matrix elements.

Due to the narrow linewidth of transitions (the linewidth of the central EPR line is 1.4 G for site 1 and 7.2 G for site 2 when **B** is parallel to ***b***, 2.6 G for site 1 and 0.6 G for site 2 when **B** is parallel to $\boldsymbol{D}_1$, 1.5 G for site 1 and 10 G for site 2 when **B** is parallel to $\boldsymbol{D}_2$), the splitting of the forbidden transitions into two lines is observed (Fig. 1). To our knowledge, it is the first time in the literature that such a splitting has been reported for rare earth elements. These splittings are due only to the quadrupole interaction **Q** and allow us to retrieve the five independent quadrupole matrix elements.

EPR measurements were performed with an *X*-band Bruker Elexsys E 500 spectrometer equipped with an Oxford Instruments variable temperature device. The crystal was mounted on a small Perspex sample holder to allow its orientation with respect to the magnetic field. Angular variations were obtained by rotating the crystal by steps of 10°. For each orientation, the positions of the allowed and forbidden transitions are determined manually from the recorded spectra. By a complete diagonalization, performed on a 16 $\times$16 matrix $[2(2I+1)\times 2(2I+1)]$, the calculated positions are compared to the experimental ones and the spin-Hamiltonian parameters are determined by minimizing the following rms_{norm} parameter taken as the figure of merit for the simulation:

$$\mathrm{rms}_{norm} = \left[\frac{1}{N-11}\sum_{i=1}^{N}\left(\frac{B_i^{expt}-B_i^{calc}}{\mathcal{E}_i}\right)^2\right]^{1/2} = \left(\frac{1}{N-11}\chi^2\right)^{1/2} \quad (3)$$

where B_i^{expt} and B_i^{calc} are the experimental and calculated magnetic field positions. χ^2 is the χ^2 statistic. To get a quantitative measure of the goodness of fit, errors (ϵ_i) have to be taken into account. For each experimental position, the errors are determined by assuming an ±1° accuracy for crystal orientations. The subscript "norm" emphasizes the use of normalized experimental data (i.e., by taking their errors explicitly into account). Fitting normalized data is necessary to ensure that positions measured with the same accuracy have the same weight in the fit. The sum runs from 1 to *N* where *N* is the number of experimental data points. To optimize the 11 parameters corresponding to the hyperfine and quadrupole interactions, 1109 and 1059 experimental positions are used for sites 1 and 2, respectively.

The fitting procedure is performed in two steps. To first obtain a set of starting spin-Hamiltonian parameters, the allowed hyperfine transitions are fitted by only taking into account the hyperfine interaction **A**. The quadrupole splitting is then fitted by fixing these previous **A** values and varying the quadrupole **Q** interaction. This procedure is equivalent to analyzing the EPR spectra by a perturbative approach. Then, with this starting set of parameters, the complete fitting procedure is performed. The positions of the allowed transitions and of the quadrupole splittings are simulated by taking into account both **A** and **Q** interactions. In the spin Hamiltonian of Eq. (2), we consider the nuclear Zeeman interaction. It does not influence the position of the allowed and forbidden transitions but it influences their intensities. It is of particular importance if one wants to reproduce the experimental EPR spectra. A home-made program based on MATLAB software is used for the simulation.

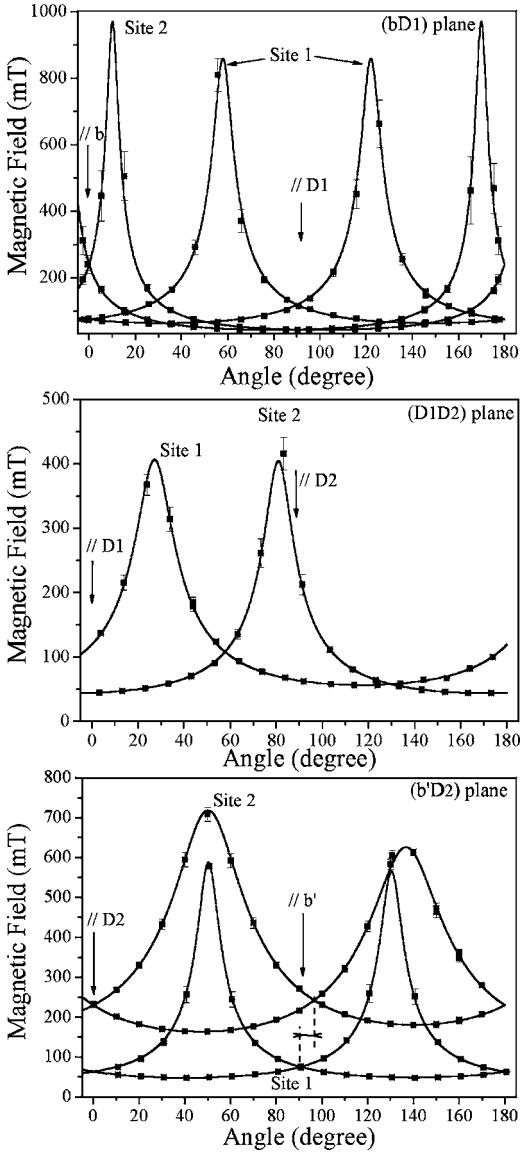

FIG. 2. Angular variation of the position (in mT) of the central line of the EPR spectra of Er^{3+} in Y_2SiO_5. The magnetic field **B** varies in three orthogonal crystallographic planes: $(\boldsymbol{b},\boldsymbol{D}_1)$, $(\boldsymbol{D}_1,\boldsymbol{D}_2)$ and $(\boldsymbol{b}',\boldsymbol{D}_2)$. See text for definition of $\boldsymbol{b}'$. The two crystallographic sites as well as the inequivalent magnetic sites are shown. Calculated curves using Eq. (1) are represented by solid lines.

III. RESULTS AND DISCUSSION

A. Electronic Zeeman interaction study

The determination of the electronic Zeeman interaction is performed by following the angular variations of the magnetic field position of the central EPR line of sites 1 and 2 and by diagonalization of the Hamiltonian of Eq. (1). Figure 2 gathers the angular variations in the three orthogonal planes as well as the calculated curves. When the magnetic field **B** has an arbitrary orientation, each site splits into two magnetic inequivalent sites. Indeed, in Y_2SiO_5, for each crystallographic site, there are four sites with different orientation in the primitive cell related to each other by a C_2 axis parallel to the $\boldsymbol{b}$ axis and an inversion operation. The sites related by the inversion operation give the same EPR signal whereas the sites related by the C_2 axis give two EPR signals for a general orientation of the magnetic field. In the $(\boldsymbol{b},\boldsymbol{D}_1)$ plane, when the magnetic field is parallel to the $\boldsymbol{b}$ or to the $\boldsymbol{D}_1$ axis, only two different EPR signals are observed, corresponding to the two different crystallographic sites; the magnetic inequivalency disappears. When the magnetic field deviates from these axes, each EPR signal splits into two magnetically inequivalent signals related by the C_2 axis. These two inequivalent sites have the same angular variations with the same extrema (Fig. 2). We take into account in the simulation this property of symmetry by applying to the Hamiltonian of Eq. (1) the C_2 symmetry operation. As the C_2 axis is perpendicular to the $(\boldsymbol{D}_1\boldsymbol{D}_2)$ plane, each site gives only one EPR signal in this plane (Fig. 2). In the $(\boldsymbol{b},\boldsymbol{D}_2)$ plane (Fig. 2), when **B** is parallel to the $\boldsymbol{D}_2$ axis, each site gives only one signal. However at 90° from $\boldsymbol{D}_2$, the signals are not superimposed. Contrary to what it is observed in the $(\boldsymbol{b},\boldsymbol{D}_1)$ plane, the angular variations of each inequivalent site are slightly different with different extrema. This effect, which is clearly seen for site 2 (Fig. 2), indicates that we are not exactly in the $(\boldsymbol{b},\boldsymbol{D}_2)$ plane but rather in a $(\boldsymbol{b}',\boldsymbol{D}_2)$ plane. We have simulated independently site 1 and site 2 and we have found for each site the same angle of misalignment: the $\boldsymbol{b}'$ axis is at 1.1° from the $\boldsymbol{b}$ axis in the $(\boldsymbol{b},\boldsymbol{D}_1)$ plane. This angle can be attributed to an error in the facet orientation of the crystal or to a slight misalignment of the crystal with respect to the magnetic field direction. This angle is taken into account in the following simulations.

From the simulations of the angular variations of the EPR central line, we have built the following matrices for the electronic Zeeman interaction:

$$g_1 = \begin{pmatrix} 2.92 & -3.08 & -3.68 \\ -3.08 & 8.19 & 5.96 \\ -3.68 & 5.96 & 5.52 \end{pmatrix}_{(D_1,D_2,b)} \quad (4)$$

for site 1 and

TABLE I. Principal values and Euler angles of the g factor of Er^{3+} ions in Y_2SiO_5 for sites 1 and 2.

	Euler angles (deg)		
Principal values	α	β	γ
	Site 1		
$\lvert g_x\rvert = 0.00(5)$			
$\lvert g_y\rvert = 1.79(3)$	207(1)	53(1)	247(1)
$\lvert g_z\rvert = 14.83(1)$			
	Site 2		
$\lvert g_x\rvert = 0.55(5)$			
$\lvert g_y\rvert = 1.70(3)$	261(1)	100(1)	103(1)
$\lvert g_z\rvert = 15.54(1)$			

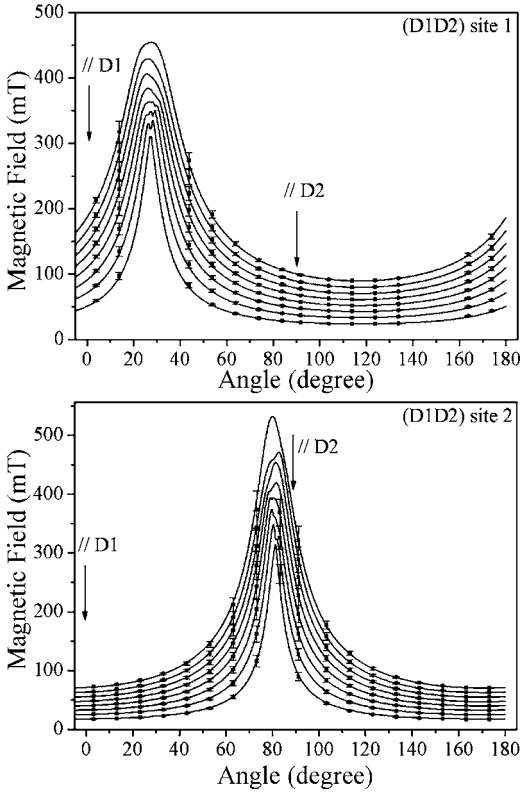

FIG. 3. Angular variation of the positions (in mT) of the eight allowed hyperfine transitions for Er^{3+} in Y_2SiO_5. The magnetic field **B** varies in the $(\boldsymbol{D}_1,\boldsymbol{D}_2)$ plane. The two crystallographic sites are shown. Calculated curves are represented by solid lines.

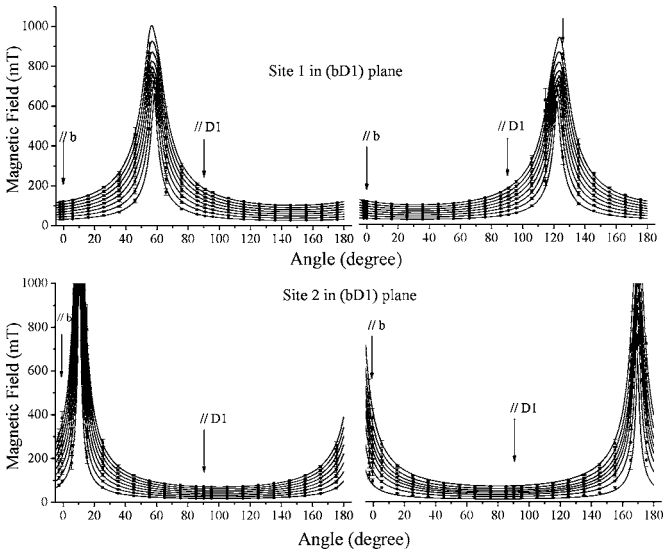

FIG. 4. Angular variation of the positions (in mT) of the eight allowed hyperfine transitions for Er^{3+} in Y_2SiO_5. The magnetic field **B** varies in the $(\boldsymbol{b},\boldsymbol{D}_1)$ plane. The two crystallographic sites are shown. Calculated curves are represented by solid lines.

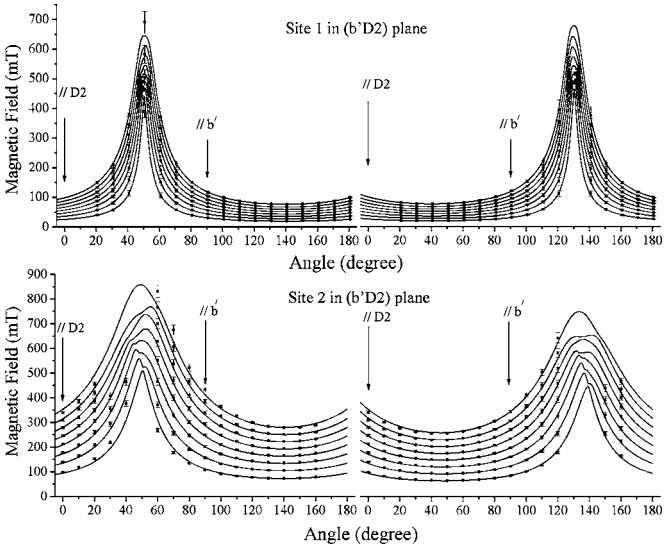

FIG. 5. Angular variation of the positions (in mT) of the eight allowed hyperfine transitions for Er^{3+} in Y_2SiO_5. The magnetic field **B** varies in the $(\boldsymbol{b}',\boldsymbol{D}_2)$ plane. See text for definition of $\boldsymbol{b}'$. The two crystallographic sites are shown. Calculated curves are represented by solid lines.

$$g_2 = \begin{pmatrix} 14.75 & -2.02 & 2.62 \\ -2.02 & 1.89 & -0.93 \\ 2.62 & -0.93 & 0.05 \end{pmatrix}_{(D_1,D_2,b)} \tag{5}$$

for site 2. After diagonalization, the principal **g** values and the Euler angles α, β, and γ of the principal axes with respect to the crystallographic axes $(\boldsymbol{D}_1,\boldsymbol{D}_2,\boldsymbol{b})$ are calculated. The results are given in Table I. Since the trace of a tensor is invariant with respect to rotations, the relative signs of the principal **g** values are deduced from the diagonalization of matrices of Eqs. (4) and (5). For site 1, the principal g values have the same sign and for site 2, the g_x value and the g_y, g_z values have opposite signs.

Our values agree with the **g** values given in Ref. 22 where only the maximum and the minimum **g** values were determined because the authors could not investigate the complete angular dependence of the resonances with respect to the magnetic field. They found a maximum value of 14.80±0.01 and 15.46±0.01 for sites 1 and 2, respectively; and a minimum **g** value smaller than 0.8 for both sites. Some small discrepancies are found with Ref. 14 probably due to small misalignment of the crystal in their experiments. As we can see from Table I, the principal axes are not oriented along the optical axes. The errors are given in parenthesis. For example, the Euler angles are given in degrees with a ±1° error.

B. Hyperfine and quadrupole interactions study

The angular variations of the eight allowed hyperfine transitions are shown in Figs. 3–5 with the calculated curves using the Hamiltonian of Eq. (2). For the sake of clarity, in the $(\boldsymbol{b},\boldsymbol{D}_1)$ and $(\boldsymbol{b}',\boldsymbol{D}_2)$ planes, the angular variations of the magnetically inequivalent sites are shown on different figures. For some magnetic field orientations and in particular

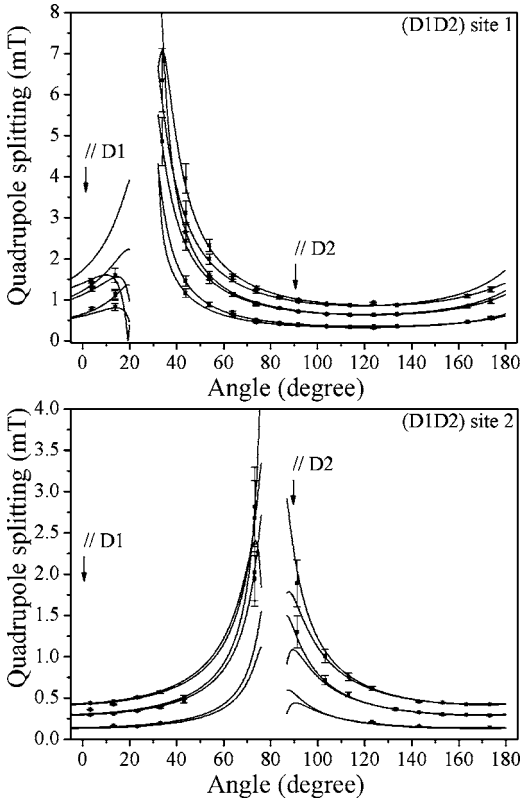

FIG. 6. Angular variation of the six quadrupole splittings (in mT) of forbidden hyperfine transitions for Er^{3+} in Y_2SiO_5. The magnetic field **B** varies in the $(\boldsymbol{D}_1,\boldsymbol{D}_2)$ plane. The two crystallographic sites are shown. Calculated curves are represented by solid lines.

when the EPR signal is going toward high magnetic field, we could not obtain accurate experimental data. For these orientations, it was not possible to distinguish between the allowed and forbidden transitions. Their intensities become equivalent and the allowed transitions were not longer equally spaced, contrary to the spectra shown in Fig. 1. These behaviors are the combination of two effects: (i) for some orientations, the quadrupole interaction is of the same order of magnitude of the hyperfine interaction and (ii) the hyperfine and quadrupole principal axes are not coincident.[15] Indeed, if we try to simulate the positions of the allowed transitions by considering the quadrupole interaction as a perturbation of the hyperfine interaction, we find a good agreement between the experimental points and the calculated ones when the EPR signals are in the low-field part of the spectra. However, when the signals are going towards the high-magnetic-field part of the EPR spectral range, the agreement is poor with at least 10% discrepancy between the experimental and the calculated curves. Figures 6–8 gather the six quadrupole splittings of the forbidden transitions as function of the magnetic field orientation with the corresponding calculated curves. For sake of clarity, some part of the calculated curves are not shown. By fitting simultaneously the positions of the allowed transitions and the quadrupole splittings we have built the following matrices for the **A** and **Q** interactions:

$$\mathbf{A}_1 = \begin{pmatrix} 69.35 & -580.73 & -248.83 \\ -580.73 & 696.30 & 682.49 \\ -248.83 & 682.49 & 495.54 \end{pmatrix}_{(D_1,D_2,b)}, \quad (6)$$

$$\mathbf{Q}_1 = \begin{pmatrix} 21.40 & -8.18 & -15.27 \\ -8.18 & 3.79 & 0.60 \\ -15.27 & 0.60 & -25.20 \end{pmatrix}_{(D_1,D_2,b)}, \quad (7)$$

for site 1 and for site 2

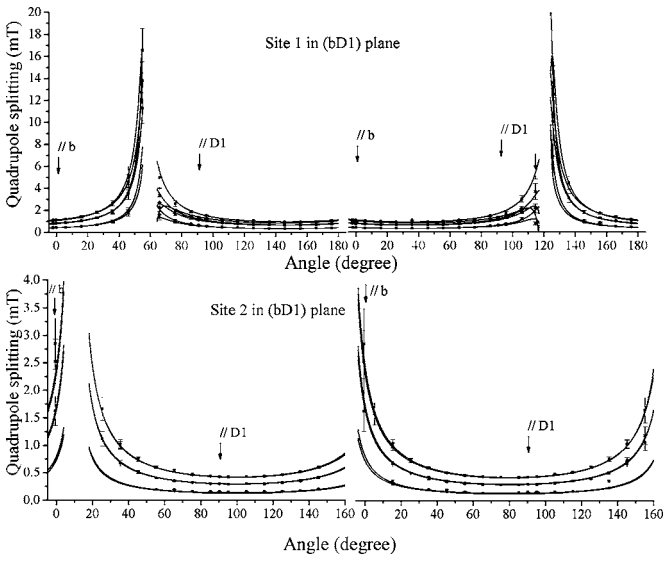

FIG. 7. Angular variation of the six quadrupole splittings (in mT) of forbidden hyperfine transitions for Er^{3+} in Y_2SiO_5. The magnetic field **B** varies in the $(\boldsymbol{b},\boldsymbol{D}_1)$ plane. The two crystallographic sites are shown. Calculated curves are represented by solid lines.

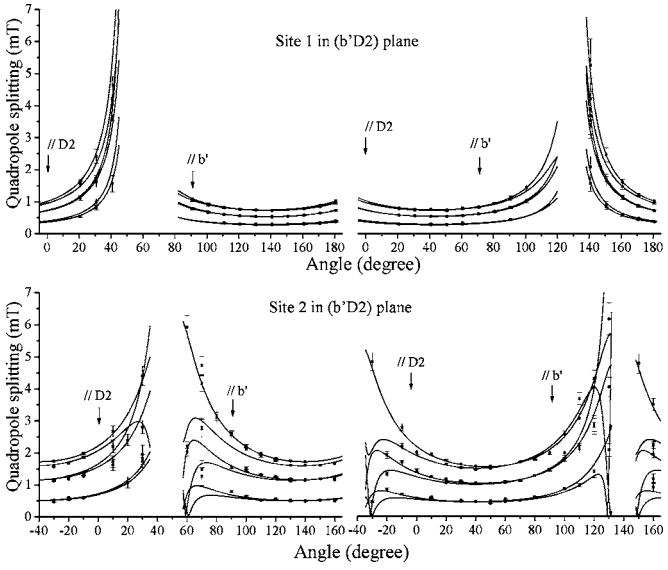

FIG. 8. Angular variation of the six quadrupole splittings (in mT) of forbidden hyperfine transitions for Er^{3+} in Y_2SiO_5. The magnetic field **B** varies in the $(\boldsymbol{b}',\mathbf{D}_2)$ plane. See text for definition of $\boldsymbol{b}'$. The two crystallographic sites are shown. Calculated curves are represented by solid lines.

TABLE II. Principal values and Euler angles of the hyperfine and quadrupole interactions of Er^{3+} ions in Y_2SiO_5 for sites 1 and 2.

A interaction				*Q* interaction			
Principal values (MHz)	Euler angles (deg) α	β	γ	Principal values (MHz)	Euler angles (deg) α	β	γ
Site 1							
$\lvert A_x\rvert$=43.6(3)				$\lvert Q_x\rvert$=28.55(3)			
$\lvert A_y\rvert$=319.1(3)	208(1)	55(1)	249(1)	$\lvert Q_y\rvert$=1.29(3)	100(1)	17(1)	117(1)
$\lvert A_z\rvert$=1536.7(2)				$\lvert Q_z\rvert$=29.85(3)			
Site 2							
$\lvert A_x\rvert$=6.3(3)				$\lvert Q_x\rvert$=56.9(1)			
$\lvert A_y\rvert$=398(3)	264(1)	95(1)	137(1)	$\lvert Q_y\rvert$=2.7(1)	287(1)	27(1)	358(1)
$\lvert A_z\rvert$=1555(2)				$\lvert Q_z\rvert$=59.6(1)			

$$\mathbf{A}_2 = \begin{pmatrix} -1521.40 & 178.11 & -141.76 \\ 178.11 & 172.09 & 212.54 \\ -141.76 & 212.54 & 199.01 \end{pmatrix}_{(D_1,D_2,b)}, \quad (8)$$

$$\mathbf{Q}_2 = \begin{pmatrix} -3.50 & -19.84 & 24.22 \\ -19.84 & 50.40 & 6.73 \\ 24.22 & 6.73 & -46.90 \end{pmatrix}_{(D_1,D_2,b)}. \quad (9)$$

A and **Q** are given in megahertz. On 1109 and 1059 experimental positions, we found a rms_{norm} value of 0.9288 and 2.0319 for sites 1 and 2, respectively. The rms_{norm} value is higher for site 2 than for site 1 because in site 2 we probably underestimate the errors. Indeed, in each plane, the position of the EPR signal attributed to site 2 is always more sensitive to a misalignment of the crystal with respect to the magnetic field direction as we have already seen in Fig. 2 for the $(\boldsymbol{b}',\boldsymbol{D}_2)$ plane. However these errors are difficult to estimate, we have thus decided to keep this rms_{norm} value for site 2. As a conclusion, the higher value of rms_{norm} for site 2 reveals a higher sensitivity of the EPR signal positions to the magnetic field orientation.

After diagonalization of matrices of Eqs. (6)–(9), the principal **A** and **Q** values and the Euler angles α, β, and γ of the principal axes with respect to the crystallographic axes $(\boldsymbol{D}_1,\boldsymbol{D}_2,\boldsymbol{b})$ are calculated. The results are given in Table II and the orientation of the principal axes of the different interactions are shown in Fig. 9. The errors are obtained from the estimated covariance matrix of the standard errors in the 11 fitted parameters by taking the square root of the diagonal elements of this matrix. The covariance matrix is obtained from the Hessian matrix as described in Ref. 23.

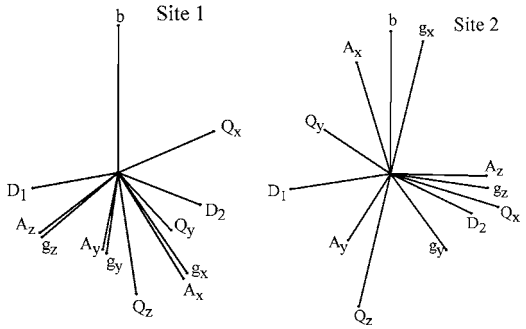

FIG. 9. Orientations of the principal axes of the **g**, **A**, and **Q** interactions with respect to the (D_1,D_2,b) axis set for sites 1 and 2 of Er^{3+} in Y_2SiO_5.

From the Euler angles, we determine by a scalar product, the angles between the principal axes of the different interactions. For site 1 and from Tables I and II, we find that the **g** and **A** interactions are quasicoincident with the g_x, g_y, and g_z principal axes oriented at 3.2°, 2.4°, and 2.3° with respect to the A_x, A_y, and A_z principal axes (Fig. 9). The quadrupole interaction **Q** is not coincident with the hyperfine interaction **A**. The A_x, A_y, and A_z principal axes are oriented at 66.1°, 33.9°, and 62° with respect to the Q_x, Q_y, and Q_z principal axes.

For site 2, the g_z principal axis is nearly coincident with the A_z component with an angle of 5.3° (Fig. 9). The g_x and g_y principal axes are oriented at 60.7°, and 119.6° with respect to the A_x and A_y principal axes. The A_x, A_y, and A_z principal axes are oriented at 129.9°, 122.3°, and 109.2° with respect to the Q_x, Q_y, and Q_z principal axes.

For site 1, the A_y value and the A_x, A_z values have opposite signs; the Q_z value and the Q_x, Q_y values have opposite signs. For site 2, the A_z value and the A_x, A_y values have opposite signs; the Q_z value and the Q_x, Q_y values have opposite signs.

To validate our set of spin-Hamiltonian parameters, two tests have been performed. First, we check if the minimum found by our program, which minimized the difference between the experimental and calculated magnetic field positions, was true. We have repeated the simulation several times by generating random sets of initial parameters. The program always converges to the same final set of spin-Hamiltonian parameters. A second test has been performed by testing the wave functions obtained from the diagonalization of the Hamiltonian of Eq. (2). For this, we have calculated the EPR spectrum of Er^{3+} ions for a very general orientation of the magnetic field and we have compared this

spectrum to the corresponding experimental one. For example, Fig. 1 gathers the calculated and the experimental spectra for **B** parallel to the ***b*** axis. The positions of the lines as well as their intensities are well reproduced. For each site, the relative intensities within the allowed and forbidden hyperfine patterns agree rather well with the experimental spectrum. Some differences are nevertheless observed. In particular, the forbidden transitions characterized by $\Delta M_I = \pm 2$, which appear on both sides of the allowed hyperfine transitions, are sometimes more intense in the computed spectra than in the experimental spectra. This discrepancy can have two origins. First, the linewidth of the hyperfine transitions are not the same along the whole hyperfine pattern. We try to consider this effect in the simulation. For example, for site 2, the linewidth of the lowest allowed hyperfine transition is half of the linewidth of the highest allowed hyperfine transition. Second, as the different transitions are very narrow, some scan speed or over modulation effects can still be present in our experimental spectra.

IV. CONCLUSION

We have characterized by EPR spectroscopy the hyperfine structure of the ground state of Er^{3+} ions in Y_2SiO_5 for both crystallographic sites. The low symmetry of these sites implies that the electronic Zeeman **g**, the hyperfine **A**, and the quadrupole **Q** interactions are not coincident. Contrary to what it is usually done in the literature, the spin Hamiltonian of the system cannot be treated by perturbation theory as the quadrupole interaction is for some orientations of the magnetic field of the same order of magnitude as the hyperfine interaction. A good agreement is obtained between experimental and simulated magnetic field positions and relative intensities of EPR lines. The agreement is better for site 1 than for site 2 with rms_{norm}'s of 0.9288 and 2.0319, respectively.

We can expect in this material a strong nuclear spin projections mixing which will imply an efficient three-level Λ system within the hyperfine levels as the transitions between the two legs of the Λ will be allowed. Having determined the ground state hyperfine splitting by EPR, hole burning spectroscopy will be performed to retrieve the hyperfine splitting of the excited state. EPR spectroscopy in the $^4I_{13/2}$ excited state under optical excitation in site 1 or site 2 can also be performed to obtain by an equivalent study the spin-Hamiltonian parameters of the excited state.

*Author to whom correspondence should be addressed. Electronic address: olivier-guillotn@enscp.fr

[1] R. M. Macfarlane and R. M. Shelby in *Spectroscopy of Solids Containing Rare Earth Ions*, edited by A. A. Kaplyanskii and R. M. Macfarlane (North-Holland, Amsterdam, 1987), p. 51.
[2] E. Fraval, M. J. Sellars, and J. J. Longdell, Phys. Rev. Lett. **92**, 077601 (2004).
[3] E. Fraval, M. J. Sellars, and J. J. Longdell, Phys. Rev. Lett. **95**, 030506 (2005).
[4] B. Julsgaard, J. Sherson, J. I. Cirac, J. Fiurasek, and E. S. Polzik, Nature (London) **432**, 482 (2004); T. Chanelière, D. N. Matsukevich, S. D. Jenkins, S. Y. Lan, T. A. B. Kennedy, and A. Kuzmich, *ibid.* **438**, 833 (2005); M. D. Eisaman, A. André, F. Massou, M. Fleischhauer, A. S. Zibrov, and M. D. Lukin, *ibid.* **438**, 837 (2005).
[5] H. J. Briegel, W. Dür, J. I. Cirac, and P. Zoller, Phys. Rev. Lett. **81**, 5932 (1998).
[6] M. D. Lukin, Rev. Mod. Phys. **75**, 457 (2003).
[7] D. F. Phillips, A. Fleischhauer, A. Mair, R. L. Walsworth, and M. D. Lukin, Phys. Rev. Lett. **86**, 783 (2001).
[8] A. V. Turukhin, V. S. Sudarshanam, M. S. Shahriar, J. A. Musser, B. S. Ham, and P. R. Hemmer, Phys. Rev. Lett. **88**, 023602 (2002).
[9] J. J. Longdell, E. Fraval, M. J. Sellars, and N. B. Manson, Phys. Rev. Lett. **95**, 063601 (2005).
[10] Ph. Goldner and O. Guillot-Noël, Mol. Phys. **102**, 1185 (2004).
[11] O. Guillot-Noël, Ph. Goldner, E. Antic-Fidancev, and J. L. Le Gouët, Phys. Rev. B **71**, 174409 (2005).
[12] F. de Seze, A. Louchet, V. Crozatier, I. Lorgeré, F. Bretenaker, J. L. Le Gouët, O. Guillot-Noël, and Ph. Goldner, Phys. Rev. B **73**, 085112 (2006).
[13] R. M. Macfarlane, J. Lumin. **100**, 1 (2002).
[14] T. Böttger, Ph.D. thesis, Montana State University, 2002.
[15] J. R. Pilbrow and M. R. Lowrey, Rep. Prog. Phys. **43**, 433 (1980).
[16] G. R. Asatryan and J. Rosa, Phys. Solid State **44**, 864 (2002); S. K. Misra and S. Isber, Physica B **253**, 111 (1998); S. K. Misr, S. Isber, J. A. Cappobianco, and E. Cavalli, Chem. Phys. **240**, 313 (1999); J. L. Boldu, M. M. Abraham, and L. A. Boatner, J. Chem. Phys. **86**, 5267 (1987); J. P. R. Wells, M. Yamaga, R. W. Mosses, T. P. J. Han, H. G. Gallagher, and T. Yosida, Phys. Rev. B **61**, 3905 (2000); M. T. Borowiec, A. A. Prochorov, A. D. Prochorov, V. P. Dyakonov, and H. Szymczak, J. Phys.: Condens. Matter **15**, 5113 (2003).
[17] M. H. L. Pryce, Proc. Phys. Soc., London, Sect. A **63**, 25 (1950).
[18] A. Abragam and M. H. L. Pryce, Proc. R. Soc. London, Ser. A **205**, 135 (1951).
[19] T. Böttger, C. W. Thiel, Y. Sun, and R. L. Cone, Phys. Rev. B **73**, 075101 (2006).
[20] F. K. Kneubühl, Phys. Kondens. Mater. **1**, 410 (1963).
[21] V. G. Grachev, Sov. Phys. JETP **92**, 1834 (1987).
[22] I. N. Kurkin and K. P. Chernov, Physica B & C **101**, 233 (1980).
[23] W. H. Press, B. P. Flannery, S. A. Teukolsky, and W. T. Vetterling, *Numerical Recipes in Pascal* (Cambridge University Press, New York, 1989), Chap. 14.